Cellulose (2014) 21:3303–3309
DOI 10.1007/s10570-014-0359-3

ORIGINAL PAPER

In situ phosphorus K-edge X-ray absorption spectroscopy studies of calcium–phosphate formation and transformation on the surface of bacterial cellulose nanofibers

Honglin Luo · Guangyao Xiong · Yizao Wan

Received: 8 March 2014 / Accepted: 4 July 2014 / Published online: 16 July 2014

Abstract In this work, for the first time, in situ formation and transformation process of embryo calcium phosphate (Ca–P) minerals on three-dimensional bacterial cellulose nanofibers was investigated. Combined with XRD, X-ray absorption near-edge structure results revealed that the embryo precursor was amorphous calcium phosphate which was subsequently converted to β-tricalcium phosphate, octacalcium phosphate, and finally to the more thermodynamically stable form of hydroxyapatite. The methodology reported herein may be extended to the studies of Ca–P and other minerals on various substrates.

Keywords X-ray absorption near-edge structure (XANES) spectroscopy · Calcium phosphate · Bacterial cellulose · Nanofiber

H. Luo
School of Science, East China Jiaotong University, Nanchang 330013, Jiangxi, China

H. Luo · Y. Wan (✉)
School of Materials Science and Engineering, Tianjin University, Tianjin 300072, China
e-mail: yzwantju@126.com

G. Xiong
School of Mechanical and Electrical Engineering, East China Jiaotong University, Nanchang 330013, Jiangxi, China

Introduction

Nature has evolved efficient strategies to synthesize complex mineralized structures that exhibit fascinating and precise architectures. Bone has long been considered a prime example with a very complicated hierarchical structure formed as a result of the oriented nucleation and growth of calcium phosphate (Ca–P) crystals on the type I collagen fibrils at nano scale (Weaver et al. 2012; Dimas et al. 2013). The fabrication of artificial bone-like biomaterials mimicking the natural bone has become a hot topic. As a biomimetic strategy, various polymers have been used as template to control the geometry and structure of the Ca–P to mimic those found in bones (Stupp and Braun 1997). Among them the polysaccharide cellulose has been believed to be a promising candidate template due to its biological and mechanical properties compatible to hard and soft tissue (Hofmann et al. 2006), abundance and renewability, and abundant reactive hydroxyl groups on the macromolecular chains, which allow various surface modifications to favor Ca–P formation (Li et al. 2012). To date, various cellulose and cellulose derivates in the form of electrospun fibers (Hayashi et al. 2009), cloth (Rhee and Tanaka 2000), fabrics (Higashi and Kondo 2012), hydrogels (Hofmann et al. 2006; Granja et al. 2001; Hutchens et al. 2006) have been used as templates for Ca–P deposition. Unlike those plant-derived cellulose materials, bacterial cellulose (BC), synthesized by nonpathogenic microbial strains such as

Gluconacetobacter, shows many unique characteristics. BC exhibits higher water holding capacity, higher crystallinity and polymerization, higher tensile strength, and a finer web-like network. More importantly, it has a nano-sized fiber diameter, microscopically similar to collagen nanofibers in natural tissues (Bäckdahl et al. 2006, 2008). All these unique properties make it a promising collagen-mimicking nano-component in tissue engineering (Bäckdahl et al. 2008; Zimmermann et al. 2011). Although significant advances have been made on mineralized nanofibers (Hartgerink et al. 2001; Wan et al. 2007, 2009; Hutchens et al. 2006; Zimmermann et al. 2011; Grande et al. 2009; Cao and Mao 2007; Du et al. 2000), the growth mechanism of Ca–P on nano-sized fibers has been elusive partly due to the difficulties in in situ observation of the growth process (Onuma and Ito 1998). Indeed, in situ observation of Ca–P formation in solutions was reported by using numerous techniques such as XRD, FTIR, XPS, time-of-flight cluster static secondary ion mass spectra (ToF-SSIMS), in situ TEM and in situ AFM (Chusuei et al. 1999; De Yoreo et al. 2013; Xin et al. 2006). Notably, Gong et al. (2012) examined the formation of spicules in embryos of Strongylocentrotus purpuratus sea urchins using X-ray absorption near-edge structure (XANES).

XANES spectroscopy is a useful technique to determine the valence, oxidation state, coordination number of individual elements as well as the chemical structure of compounds (Demirldran et al. 2011). The most significant advantage of XANES is that this technique is specific to elements. The signals in a XANES spectrum, like fingerprints, represent only specific elements. Therefore, XANES has been used to examine the phase transformation, such as the transformation characteristics of biogenic Ca–P (Sato et al. 2005, 2009) and transformation of amorphous calcium carbonate (Politi et al. 2008). Nevertheless, to our best knowledge, there has been no report on using XANES for the in situ characterization of Ca–P formation and phase transformation on a three-dimensional (3D) template at nano scale, in particular during its nascent stage.

In nature, the biological apatite crystals are formed from precursors such as amorphous calcium phosphate (ACP) (Eanes et al. 1965) and calcium hydrogen phosphate dihydrate (DCPD) (Dorozhkin and Epple 2002), which are subject to phase transformation to form hydroxyapatite (HAP) or calcium-deficient hydroxyapatite (cdHAP) crystals (Hayashi et al. 2009). In order to understand the process of natural biomineralization, studies on Ca–P mineralization process have been extensively conducted either in solutions containing calcium and phosphate ions or on templates. It has been well documented that, in most cases, ACP is the first solid Ca–P phase which evolves into the crystalline phases (Combes and Rey 2010; Sugiura et al. 2011). For instance, Sugiura and co-workers reported that the initial ACP first transformed into β-tricalcium phosphate (TCP), and then into octacalcium phosphate (OCP) (Sugiura et al. 2011). ACP is said to convert directly into HAP by some authors (Abbona and Baronnet 1996; Kim et al. 2005), while others state that the transformation takes place through an intermediate like OCP (Kibalczyc et al. 1990) and subsequent HAP crystallization [9]. In the case of Ca–P deposition on BC nanofibers, previous studies indicated that OCP was the precursor of HAP. (Nge and Sugiyama 2007; Wan et al. 2009) However, the formation of ACP on 3D BC nanofibers (with a diameter of less than 100 nm, which is the lower limit of collagen fibers in bones) has not been observed (Nge and Sugiyama 2007; Wan et al. 2007). Thus, further studies are required to clarify the formation process.

The aim of this work was to determine the early formation of Ca–P minerals and their phase transformation process by capturing embryo and intermediate states of Ca–P minerals deposited on nanofibrous templates so as to provide evidence for further studies of transformation mechanisms.

Experimental

Sample preparation

The preparation and cleansing procedures of BC pellicles were identical to those described in our previous work (Wan et al. 2007). Briefly, the bacterial strain, *Acetobacter xylinum* X-2, was grown in the culture media containing 0.3 wt% green tea powder (analytical grade) and 5 wt% sucrose (analytical grade) for 7 days. The pH of the medium was adjusted to 4.5 by acetic acid. BC pellicles were purified by soaking in deionized water at 90 °C for 2 h followed by boiling in a 0.5 M NaOH solution for 15 min. The

pellicles were then washed with deionized water several times and soaked in 1 wt% NaOH for 2 days. After rinsing with deionized water until neutrality, the BC samples were stored in distilled water until required. The phosphorylation of BC was conducted by the same procedure as reported earlier (Wan et al. 2007). Briefly, BC pellicles in the form of disc were placed into a round-bottomed flask equipped with a condenser, thermometer, and nitrogen gas inlet. 200 ml of dimethyl formamide (DMF) and 15 g of urea were added to the flask. The flask was then heated to 110 °C and immediately followed by adding a solution of 19 ml of 98 % phosphoric acid (H_3PO_4) in 50 ml DMF. The suspension was further heated to 136 °C and left to reflux for an hour under gentle stirring using a magnetic stirrer and a nitrogen stream. The reaction mixture was then cooled under flowing nitrogen gas. The resulting P-BC pellicles were removed and thoroughly rinsed with deionized water to wash out the excess H_3PO_4.

In order to induce Ca–P formation, BC pellicles were immersed in 1.5 SBF (simulated body fluid) at 37 °C for predetermined periods from as short as 2 min to 3 days. As reported previously (Rhee and Tanaka 2000), the 1.5 SBF solution was prepared by dissolving reagent grade NaCl, $NaHCO_3$, KCl, $K_2HPO_4{\cdot}3H_2O$, $MgCl_2{\cdot}6H_2O$, $CaCl_2{\cdot}H_2O$, and Na_2SO_4 in deionized water. The solution was buffered to pH 7.4 with tris(hydroxymethyl) aminomethane ($(CH_2OH)_3CNH_2$) and 1 M HCl at 37 °C. The supersaturation conditions in the 1.5 SBF solutions were maintained by periodic replacement with fresh solutions. Upon completion of immersion, samples were taken out from the solution at predetermined time points, rinsed with deionized water, and finally air dried for XANES and XRD measurements.

Characterizations

SEM was conducted to observe sample morphology and microstructure. The lyophilized samples were affixed to a copper flake with carbon adhesive and sputter-coated with gold at 10 mA for 3 min. Samples were examined using a Nano 430 FE-SEM (FEI, USA) at 10 kV. The average fiber diameter of nanofibers was determined by measuring the diameter of the nanofibers at 100 different points on a SEM image, as reported by Bhattarai et al. (2005). The diameters were presented as the average ± standard deviation.

The phosphorus (P) K-edge XANES measurements of air-dried Ca–P-coated BC samples were performed at the beamline 4B7A of Beijing Synchrotron Radiation Facility (BSRF). P K-edge XANES spectra were obtained on a double-crystal monochromator (DCM) covering the energy range of 2,140–2,180 eV with an energy resolution of about 0.2 eV and the spectra were recorded in partial fluorescence yield (PFY) mode using a solid state Si(Li) detector (PGT, USA). The electron storage ring was operated at 2.5 GeV and the current was 150–250 mA. The chamber pressure was kept at 10^{-6} Torr during the measurement. Data analysis of the experimental XANES spectra was performed using the WinXAS3.1 and the reported spectra were obtained after normalization. In addition, four high-purity Ca–P minerals including ACP, TCP, OCP, and HAP purchased from chemical suppliers were used as P standards for comparison with the sample spectra. The use of standard samples was essential for the identification of the obtained XANES spectra (Sato et al. 2005, 2009). This way allows the interpretation of XANES spectra using the fingerprint method in which the XANES of the material of interest is compared with the XANES of materials of known structures (Liou et al. 2004).

The crystalline structure was studied using a Rigaku D/max 2500 X-ray diffractometer with a Cu Kα radiation ($\lambda = 0.15405$ nm) at a voltage of 40 kV and a current of 200 mA. All samples were scanned from 5° to 60° at a scan speed of 0.2°/s. The data were obtained through a MDI/JADE6 software package attached to the Rigaku XRD instrument.

Results and discussions

A representative digital camera photo, SEM image, and fiber diameter distribution of BC nanofibrous template are shown in Fig. 1. Note that the BC pellicles were whitish and translucent. SEM images clearly showed a 3D network structure. The average fiber diameter of BC was 73 ± 13 nm. As expected, the surface of phosphorylated BC was negatively charged due to the existence of large amount of –OH groups and phosphate groups ($-PO_4^{3-}$).

Figure 2 shows the P K-edge XANES spectra obtained with standard Ca–P samples of ACP, TCP, OCP, and HAP. These spectral features were consistent with those reported in literature (Eveborn et al.

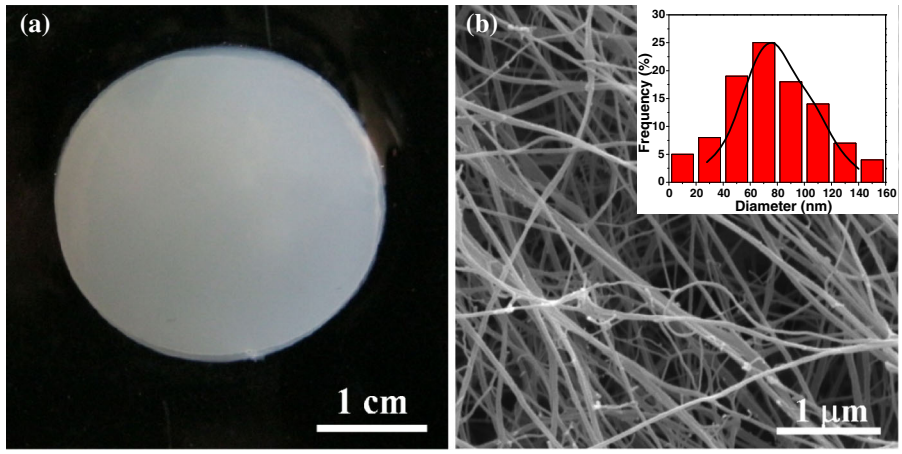

Fig. 1 Digital camera photo (**a**) and SEM image (**b**) of a representative BC nanofibrous template (*inset* showing diameter distribution of BC nanofibers)

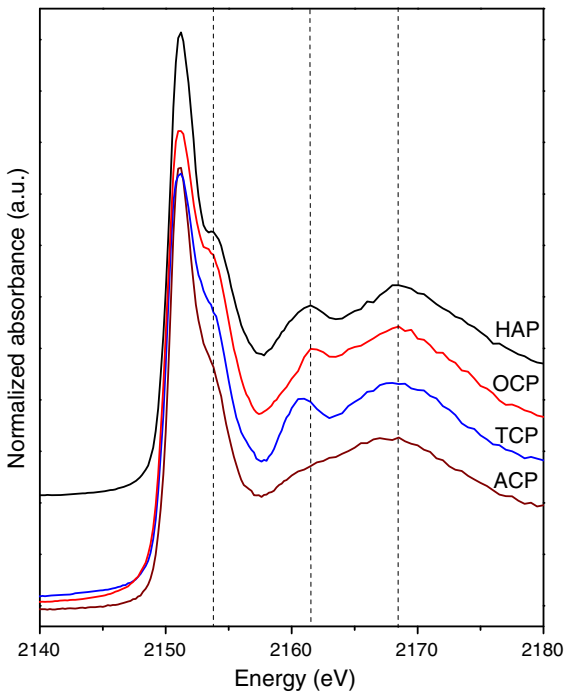

Fig. 2 Normalized P K-edge XANES spectra of various standard Ca–P minerals

2009; Sato et al. 2009). In all spectra, a peak was found at around 2,168.0 eV, which was due to oxygen oscillation and was a characteristic feature for Ca–P minerals (Sato et al. 2005, 2009). Each of the four spectra showed a shoulder at around 2,153.5 eV, which is an indication of Ca–P (Sato et al. 2009) and was in agreement with the value reported by Eveborn et al. (2009), but the shoulder seemed to be more distinctive in the order of ACP<TCP<OCP<HAP. In addition, these Ca–P minerals could be distinguished by the presence and absence of a peak at around 2,162.0 eV (Eveborn et al. 2009) [although a slight shift of this peak was observed in TCP, consistent with Sato et al. (2005)]. It should be mentioned that the spectral differences between OCP and HAP were subtle and practically it was impossible to distinguish them with XANES technique alone due to a lack of distinctive features to separate them (Eveborn et al. 2009).

The P K-edge XANES spectra of Ca–P minerals deposited on the surface of BC nanofibers after soaking in 1.5 SBF for different times are depicted in Fig. 3. Note that, as expected, there was no shoulder at 2,153.5 eV before immersion in 1.5 SBF. Interestingly, the shoulder at 2,153.5 eV could be detected after only 2 min soaking in 1.5 SBF, which confirms (comparing with Fig. 2) the presence of ACP. In other words, XANES results revealed that the precursor of Ca–P formed on BC nanofiber was ACP. This finding was consistent with the common notion of ACP being the usual initial precursor of Ca–P as mentioned above. In turn, the results confirm that the phosphorylated BC nanofiber can be an effective template for creating biomimetic materials. Furthermore, XANES also revealed that the induction period for the formation of ACP was less than 2 min. Although rapid formation of ACP in solution was reported by Sugiura et al. (2011), this is the first time to observe such short induction period in the formation of ACP on BC nanofibers. The XANES spectra shown in Fig. 3 revealed that the structure of Ca–P remained unchanged (ACP) until 3.5 h immersion in 1.5 SBF when the peak at around 2,162.0 eV was observed,

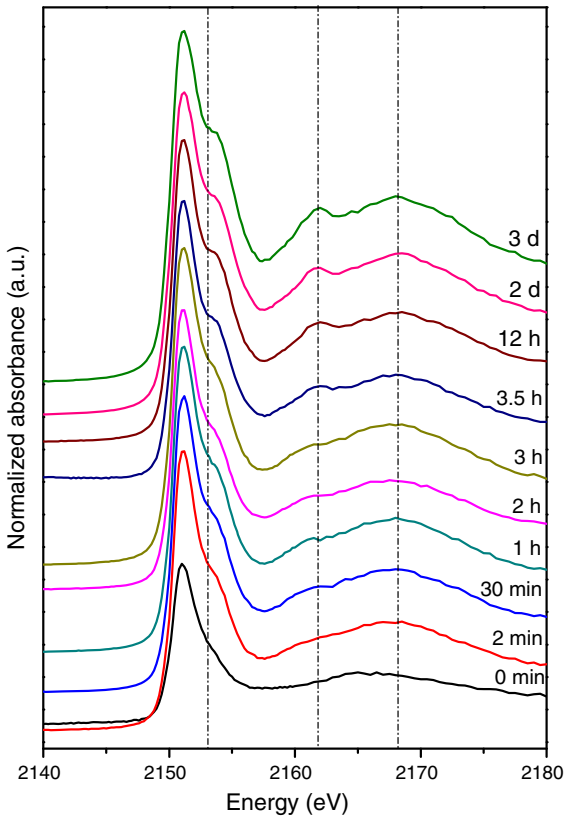

Fig. 3 P K-edge XANES spectra of Ca–P minerals deposited on the surface of BC nanofibers after soaking in 1.5 SBF for different times

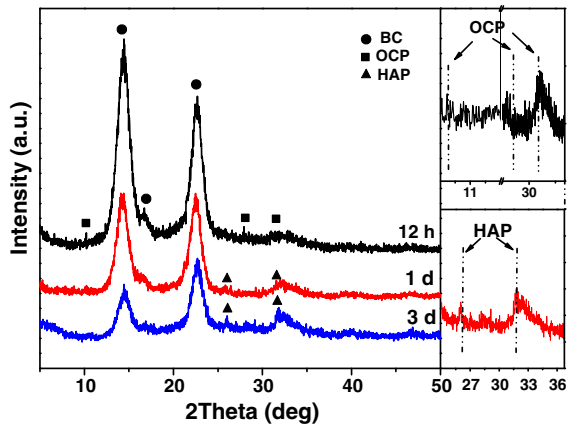

Fig. 4 XRD patterns of Ca–P minerals deposited on the surface of BC nanofibers after soaking in 1.5 SBF for different times

which indicated the transition of ACP to TCP. Furthermore, from 12 h to 3 days, the shoulder at 1,253.5 eV became more pronounced, which suggested the transition from TCP to OCP and/or HAP (comparing with Fig. 2). Nevertheless, as aforementioned, XANES was unable to tell OCP from HAP.

In order to distinguish HAP from OCP, XRD technique was adopted and the results are presented in Fig. 4. Figure 4 revealed that the mineral was OCP at 12 h immersion in 1.5 SBF and it converted to HAP after 1 day deposition. Therefore, XANES results, together with XRD findings, suggested that the embryo phase of Ca–P was ACP, which then experienced three consecutive transitions: ACP → TCP → OCP → HAP. However, to the best knowledge of the authors, none of the previous studies on Ca–P formation on BC nanofibers (Nge and Sugiyama 2007; Tolmachev and Lukasheva 2012; Wan et al. 2007, 2009) observed the formation of ACP and TCP since neither XRD nor SEM technique was able to capture the information of nascent Ca–P minerals due to various difficulties such as sample preparation and signal collection. Therefore, the use of XANES has updated our understanding on the formation of Ca–P minerals on BC nanofibers. Although the exact mechanisms of the formation of ACP precursor and thermodynamics of these phase transformations are beyond the scope of this work (which will be the focus of our future work), the findings presented in this work suggest that XANES is an effective tool to examine the formation of Ca–P minerals, in particular in the nascent stages. We believe that the use of XANES will be helpful in understanding the mechanism of biomineralization and will lead to a new strategy for mimicking biological materials.

Conclusions

In summary, the formation of embryo Ca–P minerals on 3D BC nanofibers and their transitions were studied by using XANES technique. We have shown, for the first time, that the embryo Ca–P deposited on BC nanofibers was ACP and that the transition process of Ca–P minerals on BC nanofibers was as follows: ACP → TCP → OCP → HAP. These findings have updated our understanding on the Ca–P deposition on BC. The methodology reported herein might be helpful in the study of biomineralization on other nano-sized templates.

Acknowledgments This work was supported by the National Natural Science Foundation of China (Grant No. 51172158) and the Science and Technology Support Program of Tianjin (Grant No. 11ZCKFSY01700).

References

Abbona F, Baronnet A (1996) A XRD and TEM study on the transformation of amorphous calcium phosphate in the presence of magnesium. J Cryst Growth 165(1):98–105

Bäckdahl H, Helenius G, Bodin A, Nannmark U, Johansson BR, Risberg B, Gatenholm P (2006) Mechanical properties of bacterial cellulose and interactions with smooth muscle cells. Biomaterials 27:2141–2149

Bäckdahl H, Esguerra M, Delbro D, Risberg B, Gatenholm P (2008) Engineering microporosity in bacterial cellulose scaffolds. J Tissue Eng Regen Med 2(6):320–330

Bhattarai N, Edmondson D, Veiseh O, Matsen FA, Zhang MQ (2005) Electrospun chitosan-based nanofibers and their cellular compatibility. Biomaterials 26(31):6176–6184

Cao B, Mao C (2007) Oriented nucleation of hydroxylapatite crystals on spider dragline silks. Langmuir 23(21):10701–10705

Chusuei CC, Goodman DW, Van Stipdonk MJ, Justes DR, Schweikert EA (1999) Calcium phosphate phase identification using XPS and time-of-flight cluster SIMS. Anal Chem 71(1):149–153

Combes C, Rey C (2010) Amorphous calcium phosphates: synthesis, properties and uses in biomaterials. Acta Biomater 6(9):3362–3378

De Yoreo JJ, Chung S, Friddle RW (2013) In situ atomic force microscopy as a tool for investigating interactions and assembly dynamics in biomolecular and biomineral systems. Adv Funct Mater 23:2525–2538

Demirldran H, Hu Y, Zuin L, Appathurai N, Aswath PB (2011) XANES analysis of calcium and sodium phosphates and silicates and hydroxyapatite-Bioglass (R) 45S5 co-sintered bioceramics. Mater Sci Eng C 31(2):134–143

Dimas LS, Bratzel GH, Eylon I, Buehler MJ (2013) Tough composites inspired by mineralized natural materials: computation, 3d printing, and testing. Adv Funct Mater 23(36):4629–4638

Dorozhkin SV, Epple M (2002) Biological and medical significance of calcium phosphates. Angew Chem Int Ed 41(17):3130–3146

Du C, Cui F, Zhang W, Feng Q, Zhu X, De Groot K (2000) Formation of calcium phosphate/collagen composites through mineralization of collagen matrix. J Biomed Mater Res 50(4):518–527

Eanes E, Gillessen I, Posner A (1965) Intermediate states in the precipitation of hydroxyapatite. Nature 208:365–367

Eveborn D, Gustafsson JP, Hesterberg D, Hillier S (2009) XANES speciation of P in environmental samples: an assessment of filter media for on-site wastewater treatment. Environ Sci Technol 43(17):6515–6521

Gong YUT, Killian CE, Olson IC, Appathurai NP, Amasino AL, Martin MC, Holt LJ, Wilt FH, Gilbert PUPA (2012) Phase transitions in biogenic amorphous calcium carbonate. Proc Natl Acad Sci USA 109(16):6088–6093

Grande CJ, Torres FG, Gomez CM, Carmen Bañó M (2009) Nanocomposites of bacterial cellulose/hydroxyapatite for biomedical applications. Acta Biomater 5(5):1605–1615

Granja P, Ribeiro C, De Jéso B, Baquey C, Barbosa M (2001) Mineralization of regenerated cellulose hydrogels. J Mater Sci Mater Med 12(9):785–791

Hartgerink JD, Beniash E, Stupp SI (2001) Self-assembly and mineralization of peptide-amphiphile nanofibers. Science 294(5547):1684–1688

Hayashi S, Ohkawa K, Yamamoto H, Yamaguchi M, Kimoto S, Kurata S, Shinji H (2009) Calcium phosphate crystallization on electrospun cellulose non-woven fabrics containing synthetic phosphorylated polypeptides. Macromol Mater Eng 294(5):315–322

Higashi K, Kondo T (2012) Nematic ordered cellulose templates mediating order-patterned deposition accompanied with synthesis of calcium phosphates. Cellulose 19(1):81–90

Hofmann I, Müller L, Greil P, Müller FA (2006) Calcium phosphate nucleation on cellulose fabrics. Surf Coat Technol 201(6):2392–2398

Hutchens SA, Benson RS, Evans BR, O'Neill HM, Rawn CJ (2006) Biomimetic synthesis of calcium-deficient hydroxyapatite in a natural hydrogel. Biomaterials 27(26):4661–4670

Kibalczyc W, Christoffersen J, Christoffersen M, Zielenkiewicz A, Zielenkiewicz W (1990) The effect of magnesium ions on the precipitation of calcium phosphates. J Cryst Growth 106(2):355–366

Kim S, Ryu H-S, Shin H, Jung HS, Hong KS (2005) In situ observation of hydroxyapatite nanocrystal formation from amorphous calcium phosphate in calcium-rich solutions. Mater Chem Phys 91(2):500–506

Li K, Wang J, Liu X, Xiong X, Liu H (2012) Biomimetic growth of hydroxyapatite on phosphorylated electrospun cellulose nanofibers. Carbohydr Polym 90(4):1573–1581

Liou SC, Chen SY, Lee HY, Bow JS (2004) Structural characterization of nano-sized calcium deficient apatite powders. Biomaterials 25(2):189–196

Nge TT, Sugiyama J (2007) Surface functional group dependent apatite formation on bacterial cellulose microfibrils network in a simulated body fluid. J Biomed Mater Res Part A 81A(1):124–134

Onuma K, Ito A (1998) Cluster growth model for hydroxyapatite. Chem Mater 10(11):3346–3351

Politi Y, Metzler RA, Abrecht M, Gilbert B, Wilt FH, Sagi I, Addadi L, Weiner S, Gilbert PUPA (2008) Transformation mechanism of amorphous calcium carbonate into calcite in the sea urchin larval spicule. Proc Natl Acad Sci USA 105(45):17362–17366

Rhee SH, Tanaka J (2000) Hydroxyapatite formation on cellulose cloth induced by citric acid. J Mater Sci Mater Med 11(7):449–452

Sato S, Solomon D, Hyland C, Ketterings QM, Lehmann J (2005) Phosphorus speciation in manure and manure-amended soils using XANES spectroscopy. Environ Sci Technol 39(19):7485–7491

Sato S, Neves EG, Solomon D, Liang BQ, Lehmann J (2009) Biogenic calcium phosphate transformation in soils over millennial time scales. J Soils Sediments 9(3):194–205

Stupp SI, Braun PV (1997) Molecular manipulation of microstructures: biomaterials, ceramics, and semiconductors. Science 277(5330):1242–1248

Sugiura Y, Onuma K, Kimura Y, Miura H, Tsukamoto K (2011) Morphological evolution of precipitates during transformation of amorphous calcium phosphate into octacalcium phosphate in relation to role of intermediate phase. J Cryst Growth 332(1):58–67

Tolmachev DA, Lukasheva NV (2012) Interactions binding mineral and organic phases in nanocomposites based on bacterial cellulose and calcium phosphates. Langmuir 28(37):13473–13484

Wan YZ, Huang Y, Yuan CD, Raman S, Zhu Y, Jiang HJ, He F, Gao C (2007) Biomimetic synthesis of hydroxyapatite/bacterial cellulose nanocomposites for biomedical applications. Mater Sci Eng C 27(4):855–864

Wan YZ, Gao C, Luo HL, He F, Liang H, Li XL, Wang YL (2009) Early growth of nano-sized calcium phosphate on phosphorylated bacterial cellulose nanofibers. J Nanosci Nanotechnol 9(11):6494–6500

Weaver JC, Milliron GW, Miserez A, Evans-Lutterodt K, Herrera S, Gallana I, Mershon WJ, Swanson B, Zavattieri P, DiMasi E, Kisailus D (2012) The stomatopod dactyl club: a formidable damage-tolerant biological hammer. Science 336(6086):1275–1280

Xin RL, Leng Y, Wang N (2006) In situ TEM examinations of octacalcium phosphate to hydroxyapatite transformation. J Cryst Growth 289(1):339–344

Zimmermann KA, LeBlanc JM, Sheets KT, Fox RW, Gatenholm P (2011) Biomimetic design of a bacterial cellulose/hydroxyapatite nanocomposite for bone healing applications. Mater Sci Eng C 31(1):43–49